Broadband Acoustic Cloaking within an Arbitrary Hard Cavity

Weiwei Kan, Victor M. García-Chocano, F. Cervera, Bin Liang, Xin-ye Zou, Lei-lei Yin, Jianchun Cheng, and José Sánchez-Dehesa

Phys. Rev. Applied **3**, 064019 — Published 26 June 2015

DOI: 10.1103/PhysRevApplied.3.064019

Broadband acoustic cloaking within an arbitrary hard cavity

Weiwei Kan[1,2], Victor M. García-Chocano[1], F. Cervera[2], Bin Liang[1,3],*
Xin-ye Zou[1], Lei-lei Yin[3], Jianchun Cheng[1,4],† and José Sánchez-Dehesa[2‡]
[1]*Key Laboratory of Modern Acoustics, MOE, Department of Physics, Collaborative Innovation Center for Advances Microstructures, Nanjing University, Nanjing 210093, P.R. China.*
[2]*Wave Phenomena Group, Universitat Politècnica de València, Camino de Vera s.n.(7F), ES-46022 Valencia, Spain.*
[3]*Imaging Technology Group, Beckman Institute, University of Illinois at Urban-Champaign, Urbana, Illinois 61801, USA. and*
[4]*State Key Laboratory of Acoustics, Chinese Academy of Sciences, Beijing 100190, P.R. China.*
(Dated: May 29, 2015)

This work reports the design, fabrication and experimental validation of a broadband acoustic cloak for the concealing of three-dimensional (3D) objects placed inside an open cavity with arbitrary surfaces. This 3D cavity cloak represents the acoustic analogue of a magician hat, giving the illusion that a cavity with an object is empty. Transformation acoustics has been employed to design this cavity cloak, whose parameters represents an anisotropic acoustic metamaterial. A practical realization has been made of fourteen perforated layers fabricated by drilling subwavelength holes on a 1 mm-thickness Plexiglas plates. In both simulation and experimental results, concealing of the reference object by the device is shown for airborne sound with wavelengths between 10 cm and 17 cm.

PACS numbers: 43.20.+g, 43.28.+h, 43.58.+z
Keywords: acoustic cloaking, transformation acoustics, acoustic collimation, energy funneling

I. INTRODUCTION

Acoustic cloaking defines the phenomenon of acoustic concealing of objects embedded in a gas or a fluid. The concealing is obtained when the object is surrounded by a fluid-like shell - the cloak - which bends the impinging waves around the object in such a manner that they arrive in phase at the opposite side; i.e., the sound crosses the object without being distorted by scattering events. Acoustic cloaks for two-dimensional (2D) objects were described in 2007 by Cummer and Schurig[1], who translate into the acoustics realm the design procedure employed for electromagnetic (EM) waves[2, 3]. For concealing 2D and even three-dimensional (3D) objects embedded in a gas or an inviscid fluid, the cloak acoustic parameters are obtained using transformation acoustics. The resulting materials have an inhomogeneous and anisotropic mass density, being its bulk modulus scalar but also radially dependent[1, 4]. In spite of the unavailability of these parameters in nature, research has been conducted showing the possibility of engineering acoustic metamaterials, which are artificial structures with extraordinary acoustic properties like tensorial mass density[5–8].

Though the many theoretical studies and proposals of cloaking devices based on transformation acoustics[4, 9–11] only a few experimental results have been reported so far[12]. More recently, the research on cloaking has been extended to flexural waves, where also *reduced* cloaks have been proposed[13] and experimentally reported [14]. The theoretical tool of coordinate transformation has been also extended to other areas of physics, such as heat flux, where thermal cloaking and thermal camouflage have been proposed[15, 16] and experimentally realized[16, 17].

The reason behind the difficulty of making feasible acoustic cloaks with perfect behavior is associate to the impossibility of engineering passive structures where the sound must travel with a phase velocity larger than that of the fluid background. It has been argued that such enhancement of the sound speed could be obtained by adding some physical mechanism, like temperature[18], but the designed cloak is not feasible. Another alternative consists of designing cloaks based on scattering cancellation[19–22], but the resulting cloaks have narrowband operation and the practical realizations reported till today are only axisymmetric[20, 22]

Transformation acoustics has been also applied to design ground cloaks for the concealing of 2D and 3D objects on top of flat surfaces[23, 24]. The parameters of the resulting cloaking shells consisted of positive-index anisotropic fluid-like material, which were achieved using artificial structures consisting of multiple layers of perforated plates. More recently Kan *et al.*[25] reported the demonstration of a 2D ground cloak operating in curved surfaces with cylindrical symmetry. In brief, they apply coordinate transformation to solve the problem of hiding cylindrical objects located in front of a corner made of two flat semi-infinite planes. A reduced version of the designed cloak were designed and a cloak prototype was characterized. However, the problem of rendering acoustically invisible an arbitrary 3D object placed inside an

*Electronic address: liangbin@nju.edu.cn
†Electronic address: jccheng@nju.edu.cn
‡Electronic address: jsdehesa@upv.es

open cavity with arbitrary curved surfaces (i.e., a true 3D cavity) still remains as a challenge. The resulting acoustic illusion can be considered as the analog in acoustics of the optical illusion produced by a *magician hat*.

This work reports the design and practical realization of a *magician hat* for acoustic waves. This device represents a 3D acoustic cloak allowing the concealing of 3D arbitrary objects located inside an open cavity with arbitrary boundaries. The proposed 3D device creates the illusion of an empty cavity though, in fact, it is partially occupied. The resulting 3D cloak consists of an acoustic metamaterial which is obtained using an array of perforated plates with subwavelength holes. Due to absence of resonant elements, the device operates over a wide bandwidth and it is effective for a broad range of incident angles. The fabricated device could be considered as a generalization of the reported 2D cloaks[23–25] but here we are dealing with true 3D objects surrounded with arbitrary surfaces with no ideal assumptions (like 2D spaces or infinite flat reflecting planes).

This article is organized as follows. After this introduction, Sec. II reviews the transformation technique applied to design the acoustic cavity cloak and its performance at distances near and far from the cavity aperture. Then, Sec. III presents details of the fabricated sample together with its experimental characterization. The results are discussed in Sec. IV, which analyzes results in terms of the so called visibility factor. Finally, Sec. V summarizes the main findings of this work.

II. THEORY

We have considered an open cavity consisting of a truncated cone with height 15 cm and ellipsoidal section. This cavity has non-cylindrical symmetry and could be considered as a simple example of a cavity with arbitrary shape. The semiaxes of the ellipsoid corresponding to the cavity aperture are 12 cm and 18 cm, respectively. Figure 1(a) shows a photograph of the constructed cavity.

The cloak is designed following the coordinate transformation technique. The relationships between the tensorial effective mass density ($\bar{\rho}$) and the scalar bulk modulus (B) in the virtual (v) and real (r) systems is given by $\rho'^{-1} = \mathbf{H}\bar{\rho}^{-1}\mathbf{H}^T/det(H)$ and $B^r = det(\mathbf{H})B^v$, where $\mathbf{H}$ is the Jacobian defined as $\mathbf{H} = diag\{\partial x'_1/\partial x_1, \partial y'_1/\partial y_1, \partial z'_1/\partial z_1\}$.

Since the physical space can be regarded as a compressed conformal transformation of the virtual space, the mapping between the physical and virtual spaces is specified by $x_1^r = x_1$, $y^r = y_1$, and $z^r = z_1/n_c$, where n_c is the index of compression, which can take an arbitrary value. In this work we have considered the value 2.13. $\rho_v(x, y, z)$ and $B_v(x, y, z)$ are the position dependent parameter in the chosen virtual space. Therefore, the cloak parameters are $\rho^r(x, y, z) = diag\{1/n_c, 1/n_c, n_c\}$ and $B^r(x, y, z) = B^v(x, y, z)/n_c$. Because of the symmetry of the unit cell there are only two independent density com-

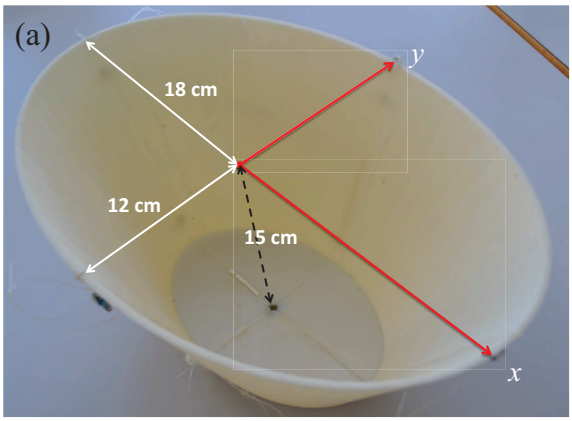

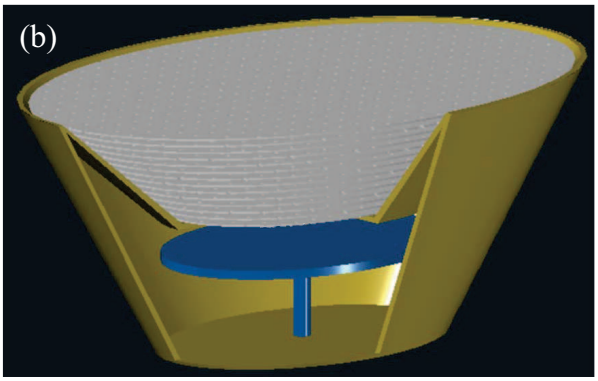

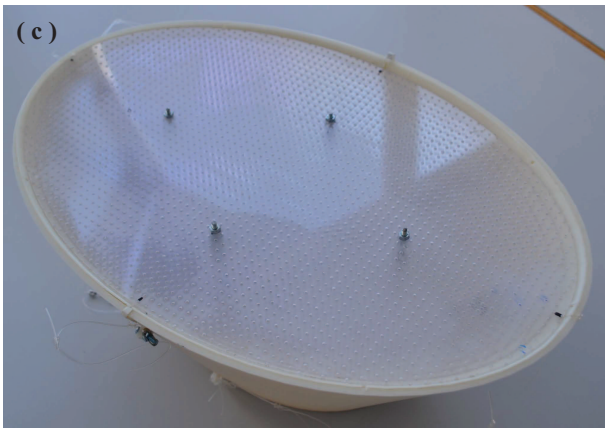

FIG. 1: (a) Photograph of the acoustic cavity manufactured using a 3D printer. It consist of a truncated cone with height 15 cm and the semi-axes of the ellipsoidal aperture has 18 cm and 12 cm, respectively. (b) Scheme of the cavity containing a 3D object (in blue) and with the metamaterial cloak on top (gray layers). (c) Photograph of cavity with the reduced cloak inserted in the cavity.

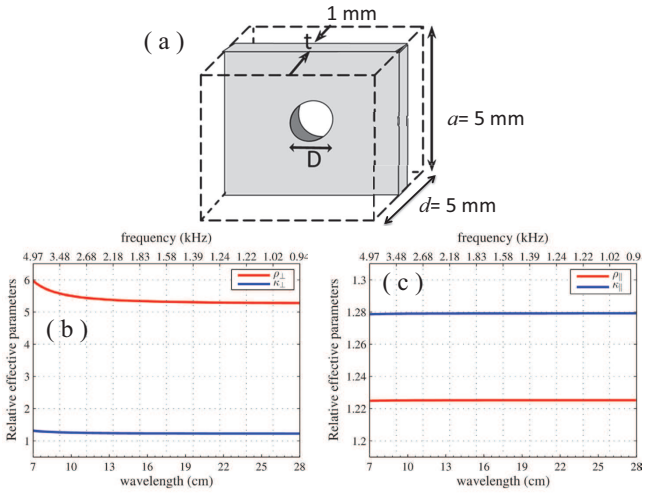

FIG. 2: Unit cell of the anisotropic structure and their effective acoustic parameters: (a) Illustration of the unit cell. (b-c) Retrieved effective parameters of the structure as a function of frequency when the wave normally impinges on the plate (b), and when the wave travels parallel to the plate (c). The red line is the effective mass density and the blue line is the bulk modulus, both parameters being normalized to the properties of air.

ponents, $\rho_{||}$ and $\rho_{\perp}$, representing the parallel and perpendicular components, respectively, to the $XY-$plane [see Fig. 1(c)].

Following the transformation procedure, the material parameters required for the perfect cloak are $\rho_{||} = 0.47\rho_0$, $\rho_{\perp} = 2.13\rho_0$ and $B = 0.47B_0$, where ρ_0 and B_0 are the mass density and bulk modulus of the surrounded background (air in this work). These parameters indicate that the cloak should be made of an anisotropic fluid with a parallel component of the density smaller than the air density. In addition, its bulk modulus must be also smaller than that of air. This type of fluid-like material, less dense and less rigid than air, is extremely difficult to engineer by passive structures. To overcome this issue we decided designing a *reduced* cloak whose parameters are augmented in the same ratio, thus becoming $\rho_{||} = 1.2\rho_0$, $\rho_{\perp} = 5.4\rho_0$ and $B = 1.2B_0$. These parameters imply that the acoustic impedance of the reduced cloak is not matched with that of air, although the phase information is conserved. Therefore, unavoidable reflections will appear between the cloak and the air not existing for the perfect cloak[18]. However the refractive index of the proposed metamaterial is not altered with respect to the original, so the resulting device will be able to create a good illusion of concealing for a given reference object.

A. Designing the artificial structure representing the reduced cloak

To achieve the required parameters of the proposed reduced cloak, we employed a layered structure consisting of fourteen perforated Plexiglas plates. Figure 1(b) shows a schematic representation of the cavity (colored in yellow) together with the inserted object (colored in blue) and the metamaterial cloak (in gray).

Each plate consists of a square lattice of subwavelength circular holes with lattice period a =5 mm, which is small enough to ensure the validation of the effective medium approximation in the range of wavelengths employed experimentally; i.e., in the domain 10 cm$\leq \lambda \leq$ 17 cm. The anisotropic unit cell is shown in Fig. 2(a), where the plate thickness t =1mm, and the hole diameter D=1.6 mm. The distance between perforated plates d =5 mm.

The effective parameters of the multilayer structure are calculated with the retrieval method proposed in Ref. [1]. The wavelength dependence of the resulting effective parameters are represented in Fig. 2(b) and 2(c), corresponding to the case where the wave impinges normally the plate and to that in which the incident wave travels along the plate, respectively. The red line is the normalized effective mass density and the blue line is the normalized bulk modulus. For the bulk modulus, it can be observed that $B_{\perp} \approx B_{||}$ and, therefore, the bulk modulus can be considered as an scalar magnitude. It is noticed that the parallel component of the effective mass density $\rho_{||}$ is much larger than the perpendicular one $\rho_{\perp}$. This structure increases the momentum in the direction perpendicular to the plates, while affect little in the direction parallel to them. It is also observed that, in the range of wavelengths experimentally studied (above λ =10 cm), the effective parameters nearly remains constant, and consequently the fabricated device will be able to work in this broad band region. For wavelengths below 10 cm the effective parameters are dispersive and the metamaterial approach is not valid.

B. Cloak performance near the cavity aperture

The scattering properties of the cloaks previously described (ideal and reduced), together with those of the empty cavity and the cavity with the object, are shown in Fig. 3, which reports the total pressure pattern on the XZ plane obtained from 3D finite element (FE) method. Numerical simulations using COMSOL Multiphysics were performed by illuminating the cavity with an incident sound with a plane wavefront perpendicular to the $z-$axis. The external boundaries of the simulation domain are non-reflective, while the boundaries of the cavity shell and the object are considered rigid. Figure 3 shows snapshots at the chosen wavelength of λ =13 cm, corresponding to the frequency f =2680 Hz (obtained by considering an air sound speed c_0 =348m/s).

Figure 3(a) depicts the field resulting from the scattering between the impinging sound and the empty cavity at the given frequency. A standing wave is observed along the $z-$axis due to reflections by the cavity boundaries, which behave as rigid surfaces. Figure 3(b) reports how the initial pattern is distorted when the reference object,

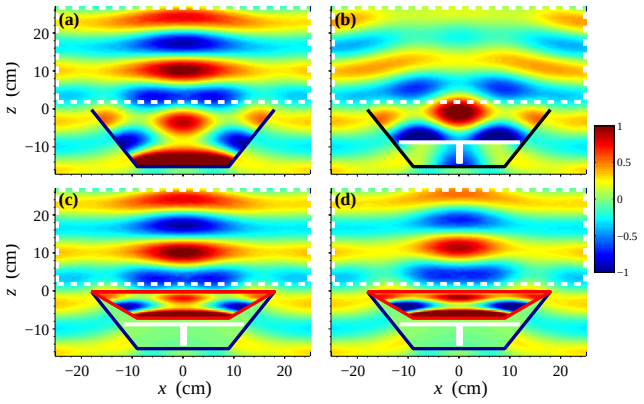

FIG. 3: (Color online) Calculated total pressure field (real part) obtained from finite-element simulations for the different configurations of the cavity: (a) empty; (b) with the object inside; (c) with the object and the ideal cloak on top; and (d) with the object and the reduced cloak. The object is represented using thick white lines while the cloak's boundaries are represented with red lines. The dashed lines enclose the area to be experimentally scanned. The impinging sound with frequency 2.68kHz has a perfect plane wave front along the $z-$axis. For animations of the instantaneous fields see Video 1.

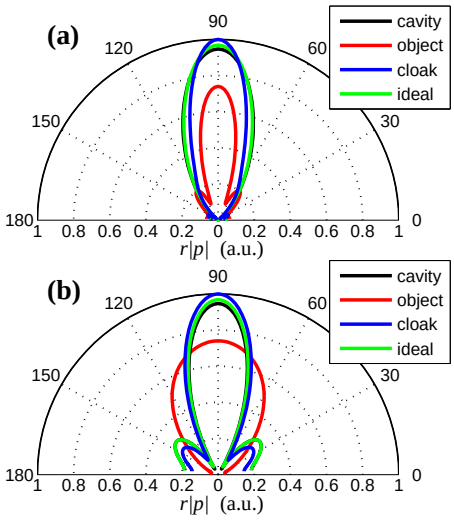

FIG. 4: Polar plots of the radiation profile calculated at the far field for the (a) XZ and (b) YZ planes. The color lines define the profiles obtained for the empty cavity (black), the cavity with a mushroom-like object (red), the cavity with the object and the perfect cloak (green), and the expected profile when the reduced cloak is considered (blue). Results are obtained with a wavelength of 13 cm (2.68 kHz)

having a mushroom-like profile, is inserted in the cavity. After covering the object with the ideal cloak, Fig. 3(c) shows that the standing wave pattern outside the cavity is perfectly recovered and, therefore, the acoustic illusion is created. Finally, in Fig. 3(d) it is observed that the standing wave profile corresponding to the reduced cloak is slightly different to that of the ideal cloak, but it is good enough for the purpose of its practical realization. Motion pictures showing the time evolution of the calculated pressure maps of the cavity, the cavity with the object and the reduced cloak for two selected frequencies, 2.68 kHz and 3.48 kHz, are presented in Videos 1 and 2, respectively. Additional frequencies were also explored confirming the wide band operation of the designed cloak devices.

We should also remark that the designed cloak operates for a broad range of impinging angles, as it is observed in Video 3, which shows the time evolution of the pressure maps obtained for an impinging wave tilted 20^o with respect to the normal.

C. Cloak performance at distances far from the aperture

The performance of the cloak at the far field has been also numerically studied and the polar plots of the radiation profiles on the XZ and YZ planes are shown in Figs. 4 and 5 for the wavelengths of 13 cm and 10cm, respectively. The radiation profiles have been calculated from the expression $r\,|p(r,\theta)|$, for $r \to \infty$. A strong distortion is observed when the profiles obtained for the empty

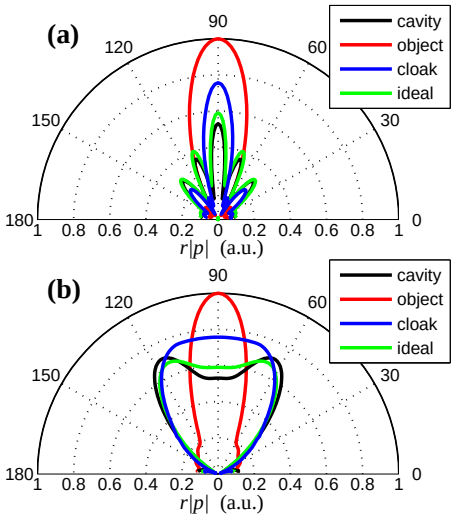

FIG. 5: Polar plots of the radiation profile calculated at the far field for the (a) XZ and (b) YZ planes. The color lines define the profiles obtained for the empty cavity (black), the cavity with a mushroom-like object (red), the cavity with the object and the perfect cloak (green), and the expected profile when the reduced cloak is considered (blue). Results are obtained with a wavelength of 10 cm (3.43 kHz)

cavity (black lines) are compared with those of the cavity with the object (red lines). However, it is remarkable that the profiles for the ideal cloak (green lines) and the reduced cloak (blue lines) are practically the same and both are similar to that of the empty cavity.

From the results shown in Figs. 4 and 5 we conclude

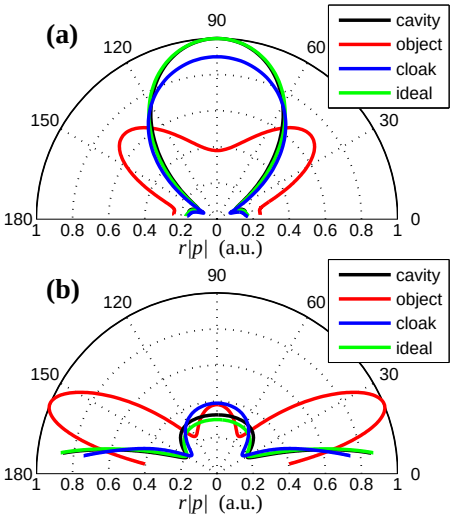

FIG. 6: Far-field radiation patterns for a viewpoint tilted 0.3π with respect to the (a) XZ and (b) YZ planes for a wave impinging on the empty cavity (black lines), the cavity with object (red lines), the ideal cloak (green lines) and the reduced cloak (blue lines. Results are obtained with a wavelength of 13 cm (2.68 kHz).

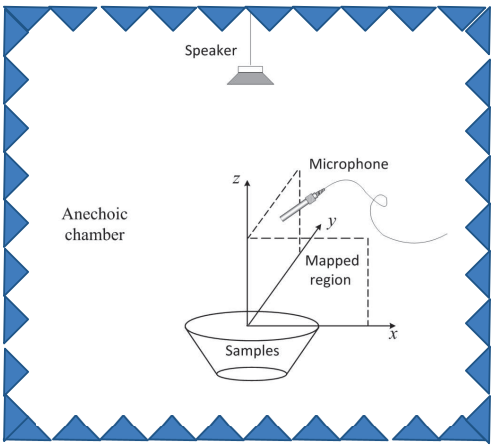

FIG. 7: Scheme of the experimental setup employed in mapping the pressure field inside the anechoic room. The $ZX-$ and $ZY-$planes together with the speaker and microphone are depicted.

that the performance of the reduced cloak is comparable with that of the ideal cloak at distances far from the cavity. Therefore, the reduced cloak is considered good enough for producing the illusion associated to a true acoustic magician hat. However, let us point out that results in Fig. 5, corresponding to a relatively high frequency (3.43 kHz), indicate that the reduced cloak does not work as well as in the case shown in Fig. 4, corresponding to a lower frequency (2.68 kHz). The are two reasons explaining this behavior. First, the effect of the impedance mismatch becomes more important for acoustic waves with shorter wavelengths. An second, the wave becomes sensitive to the parameter deviation from the ideal values for shorter wavelengths.

Profiles in Figs. 4 and 5 were calculated for the viewpoints defined by both symmetry planes XZ and YZ. Figure 6 shows now the results for viewpoints defined by planes rotated an angle of 0.3π with respect to the symmetry planes. Better contrast can be observed as the profile for the reference object (red line) is much different from the other cases (blue and black lines), which indicates that the object would be easily detected at such viewpoints without the cloak. The far-field profile of the reduced cloak (blue line) practically overlaps with that of the empty cavity and with the empty cavity, indicating that the cloak works also well under these circumstances.

III. EXPERIMENTAL

The previous theoretical findings have been experimentally verified by fabricating the cavity and the metamaterial cloak with the properties of the reduced cloak. A comprehensive acoustic characterization of the structures has been conducted inside an anechoic room as it is explained below.

First, the cavity shell has been fabricated with a 3D printer which uses ABS thermoplastic as building material. In addition, the reduced cloak was constructed using fourteen perforated Plexiglas plates whose parameters were obtained from a rigorous design procedure explained in Sect. II A. A photograph of the fabricated cavity with the cloak on top is shown in Fig. 1(c). The materials employed in the construction of the cavity and the cloak are acoustically rigid in the range of frequencies explored.

The different samples (empty cavity, cavity with the object and cavity with the object plus the cloak) were separately characterized in an anechoic chamber with dimensions $8\times6\times3$ m^3. During the measurement process a B&K 4958 microphone attached to two combined linear steppers is moved in order to perform a 2D sweep on the 50×25 cm^2 area defined in Fig. 3 with white dashed lines. The robots scan this area in the XZ and YZ planes with a spacial resolution of 1 cm. Moreover, an additional robot allows turning the sample in such a manner that its response could be measured as a function of the incident angle. The impinging wave is provided by a column loudspeaker placed at 4m from the sample and aligned with it [see Fig. 7]. A chirp consisting of a frequency sweep between 2 and 4kHz has been used as the excitation signal. Taking into account the wavelength of the emitted signals, the wavefront can be considered as

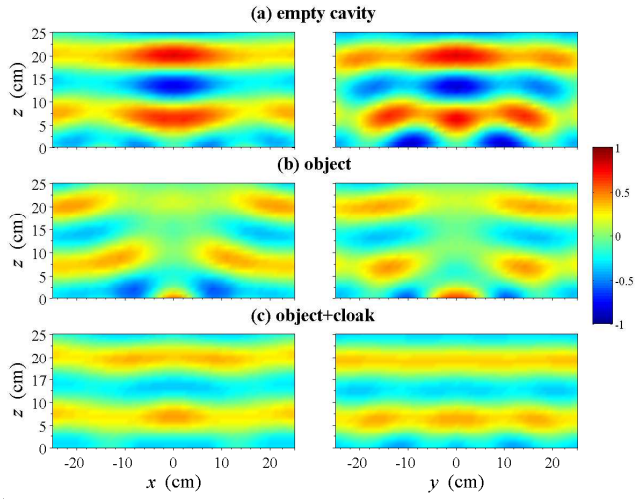

FIG. 8: (Color online) Snapshots of the pressure maps measured at 2.68 kHz. Maps on the left (right) column represent the real part of the total pressure measured on the XZ (YZ) plane for the three cases of interest: (a) Empty cavity; (b) cavity with the object, and (c) cavity with the object and the cloak. For animations of the instantaneous fields see Video 4.

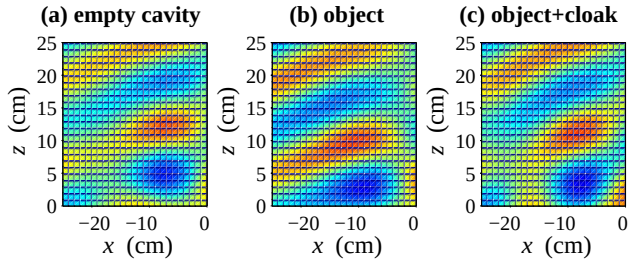

FIG. 9: (Color online) Snapshots of the pressure maps measured at 2.68 kHz (λ =13 cm) with an incident angle of 20^o. Maps represent the real part of total pressure measured on the XZ plane for: (a) Empty cavity; (b) cavity with the object, and (c) cavity with the object and the cloak. For animations of the instantaneous fields see Video 6.

plane when arriving to the samples. The amplitude and phase of the total field are obtained by processing the recorded signal through a Fourier transform. The presence of random noise has been reduced by averaging the responses of several emissions.

IV. RESULTS AND DISCUSSION

Figure 8 shows the real part of the total pressure measured in the scanned area. The 2D maps taken in both the XZ (left panels) and YZ (right panels) planes are in good agreement with FE simulations. As predicted by the simulations, the comparison between experimental data in Fig. 8(a) and Fig. 8(b) shows that a strong distortion of the field is obtained when an object is put inside the cavity. Finally, in Fig. 8(c) it is observed

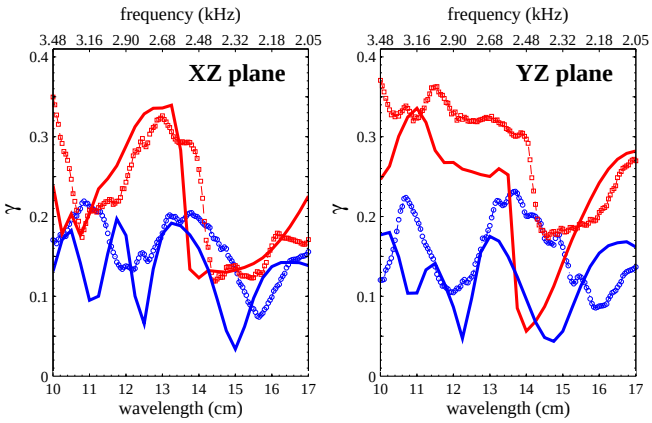

FIG. 10: (Color online) Visibility factor (γ) as a function of the wavelength calculated from the measurements (symbols) and from the finite element simulations (continuous lines). The red data correspond to the sample with the object inside the cavity while the blue data correspond to the cavity with the cloak and the object.

that the field pattern of the empty cavity is practically recovered when the cloak is added to the cavity. Motion pictures showing the time evolution of the measured pressure maps for two selected frequencies, 2.68 kHz and 3.48 kHz, are presented in Videos 4 and 5, respectively.

The comparison between pressure levels in Figs. 8(a) and 8(c) shows that some attenuation appears in the structure with the cloak. This effect is due to unavoidable losses in the metamaterial cloak and has been also observed in all the reported cloaks consisting on layers of perforated plates[14, 23–25]. In terms of pressure amplitude, we have estimated that the fabricated cloak produces a reduction of about 25% of the pressure amplitude measured without cloak. Regarding this issue, we have to remember that absorption due to viscous-thermal effects by microperforated plates is a strong and well known phenomenon[26]. For the case of perforated plates made of millimeter size holes and moderated filling fraction, as in our cloak, the absorption is much smaller but non-negligible, as has been recently proven in a different context[27].

The dependence on the impinging direction has been also verified for three different directions; 10^0, 20^o and 30^o. It has been observed that the object disturbs the 2D field pattern more weakly for increasing values of incident angles. As an example, Fig. 9 shows snapshots of the cloak performance for an incident wave tilted 20^o with respect to the normal. Video 6 shows the time evolution of the measured pressure maps. These experimental data confirm that the fabricated cloak works as a device able to conceal acoustically an object located inside a cavity with arbitrary hard boundaries and for a broad range of incident directions.

In order to quantify the cloak performance in a single number we have defined a frequency dependent *visibility*

factor γ, inspired in the one employed to characterize cloaks in free space[12, 20, 22]. For example, for the data taken on the $XZ-$plane:

$$\gamma_{XZ}(\omega) = \frac{1}{T}\int \frac{\int |Re\left[p_2(x,z) - p_1(x,z)\right]| \, dxdz}{\int \left(|p_2(x,z)| + |p_1(x,z)|\right) dxdz} e^{i\omega t} dt, \tag{1}$$

the time averaging being performed over the period T corresponding to the given angular frequency ω. The spatial integrals contain the pressures p_1 and p_2 to be compared in the selected area, and the integrals are calculated inside that area. So, γ provides a quantitative estimation of the disparity of two field maps. Note that p_1 is here chosen as the field corresponding to the empty cavity sample, which is considered the reference field. In the previously studied cloaks[12, 22] the reference field correspond to the sound wave propagating in free space. On the other hand, p_2 is the field obtained for a different sample. For the cloak sample, a value γ =0 means perfect concealing of the object. Results obtained for both XZ and YZ planes are depicted in Fig.10, where the wavelength dependence of the visibility factors obtained from the measurements (symbols) are compared with those obtained from FE simulations (continuous lines). It is noticed that the parameter experimentally obtained basically reproduce the behavior of the ones numerically calculated. Though the fabricated cloak does not provide the acoustic parameters of the perfect cloak, the resulting device (blue data) significantly reduces the visibility factor with respect to that of the object (red data). It is also observed that γ for the cloak device presents oscillations as a function of the wavelength. This effect is due to the impedance mismatch between cloak and air produced by the reduced set of acoustic parameters[18]. The averaged values of γ in the analyzed frequency domain are 0.12 and 0.15, corresponding to simulations and measurements, respectively. These values, which are only slightly above from the zero level (defining perfect concealing) support our claim of the wide band operation of our reported cloak.

V. SUMMARY

In summary, we have shown that 3D objects located inside a cavity with arbitrary curved surfaces can be efficiently concealed from an external sound using a cloak designed with transformation acoustics. The designed cloak consists of an acoustic metamaterial with an anisotropic mass density, which has been engineered with a stack of perforated layers with subwavelength holes. Though the fabricated cloak has a simplified set of acoustic parameters, its performance shows an broadband operation for a large range of incident directions. The functionality here described represents the acoustic analogue of a magician hat, creating the illusion that a cavity filled with a 3D object is completely empty.

W.W.K., B.L. and J.C.C. acknowledge support by the National Basic Research Program of China (973 Program) (Grant Nos. 2010CB327803 and 2012CB921504), National Natural Science Foundation of China (Grant Nos. 11174138, 11174139, 11222442, 81127901, and 11274168), NCET-12-0254, A Project Funded by the Priority Academic Program Development of Jiangsu Higher Education Institutions and a program supported by China Scholarship Council (CSC). W.W.K. was also supported by the program for outstanding PhD students of Nanjing University. V.M.G.-C, F.C. and J. S.-D. acknowledge financial support from the USA Office of Naval Research under grant No. N00014-12-1-0216 and from the Spanish Ministerio de Economía y Competitividad under grant No. TEC2010-19751.

Appendix

The dynamics of the total pressure field are demonstrated by videos from sequences of snapshots taken along one period. Each image is obtained by calculating or measuring the image at specific time intervals within a period.

Video 1: Motion picture showing the calculated pressure map on the XY plane for: (a) the empty cavity, (b) the cavity with a mushroom-like object, and (c) the cavity with the object and the cloak. The sound impinges the cavity at normal incidence and has a frequency of 2.68 kHz (λ =13 cm).

Video 2: Motion picture showing the calculated pressure field pattern in the XY plane for: (a) the empty cavity, (b) the cavity with a mushroom-like object, and (c) the cavity with the object and the cloak. The sound impinges the cavity at normal incidence and has a frequency of 3.48 kHz (λ =10 cm).

Video 3: Motion picture showing the calculated pressure map on the XY plane for: (a) the empty cavity; (b) the cavity with the object, and (c) the cavity with the object and the cloak. The sound has a frequency of 2.68 kHz (λ =13cm) and the impinging angle is 20 degrees.

Video 4: Motion picture showing the experimentally measured pressure map on the XY plane for: (a) the empty cavity, (b) the cavity with a mushroom-like object, and (c) the cavity with the object and the cloak. The sound impinges the cavity at normal incidence and has a frequency of 2.68 kHz (λ =13 cm).

Video 5:Motion picture showing the experimentally measured pressure map on the XY plane for: (a) the empty cavity, (b) the cavity with a mushroom-like object, and (c) the cavity with the object and the cloak. The sound impinges the cavity at normal incidence and has a frequency of 3.48 kHz (λ =10 cm).

Video 6: Motion picture showing the experimentally measured pressure map on the XY plane for: (a) the empty cavity; (b) the cavity with the object, and (c) the cavity with the object and the cloak. The sound has a frequency of 2.68 kHz (λ =13cm) and the impinging angle is 20 degrees.

[1] S. Cummer and D. Schurig, One path to acoustic cloaking, New J. Phys. **9**, 45 (2007).

[2] U. Leonhardt, Optical conformal mapping, Science **10**, 1777 (2006).

[3] J. Pendry, D. Schurig, and D. R. Smith, Controlling electromagnetic fields, Science **10**, 1780 (2006).

[4] H. Chen and C. Chan, Acoustic cloaking in three dimensions using acoustic metamaterials, Appl. Phys. Lett. **91**, 183518 (2007).

[5] B. Popa and S. A. Cummer, Design and characterization of broadband acoustic composite metamaterials, Phys. Rev. B **80**, 174303 (2009).

[6] D. Torrent and J. Sánchez-Dehesa, Anisotropic Mass Density by Radially Periodic Fluid Structures, Phys. Rev. Lett. **105**, 174301 (2010).

[7] I. Spiousas, D. Torrent, and J. Sánchez-Dehesa, Experimental realization of broadband tunable resonators based on anisotropic metafluids, Appl. Phys. Lett. **98**, 244102 (2011).

[8] J. Christensen and F. J. Garcia de Abajo, Anisotropic Metamaterials for Full Control of Acoustic Waves, Phys. Rev. Lett. **108**, 124301 (2012).

[9] D. Torrent and J. Sánchez-Dehesa, Acoustic resonances in two-dimensional radial sonic crystal shells, New J. Phys. **10**, 063015 (2008).

[10] A. Norris, Acoustic metafluids, J. Acous. Soc. Am. **125**, 839 (2009).

[11] X. Zhu, B. Liang, W. Kan, X. Zhou, and J. Cheng, Acoustic cloaking by a superlens with single negative materials, Phys. Rev. Lett. **106**, 014301 (2011).

[12] S. Zhang, C. Xia, and N. Fang, Broadband acoustic cloak, Phys. Rev. Lett. **106**, 024301 (2011).

[13] M. Farhat, S. Guenneau, and S. Enoch, Ultrabroadband Elastic Cloaking in Thin Plates, Phys. Rev. Lett. **103**, 024301 (2009).

[14] N. Stenger, M. Wilhem, and M. Wegener, Experiments on Elastic Cloaking in Thin Plates, Phys. Rev. Lett. **108**, 014301 (2012).

[15] S. Guenneau, C. Amra, and D. Veynante, Transformation thermodynamics: cloaking and concentrating heat flux, Opt. Express **20**, 8207 (2012).

[16] T. Han, X. Bai, J. Thong, B. Li, and C. Qiu, Full Control and Manipulation of Heat Signatures: Cloaking, Camouflage and Thermal Metamaterials, Adv. Mat. **26**, 93904 (2014).

[17] R. Schittny, M. Kadic, S. Guenneau, and M. Wegener, Experiments on Transformation Thermodynamics: Molding the Flow of Heat, Phys. Rev. Lett. **110**, 195901 (2013).

[18] V. M. García-Chocano, D. Torrent, and J. Sánchez-Dehesa, Reduced cloaks by temperature gradients, Appl. Phys. Lett. **101**, 084103 (2011).

[19] M. D. Guild, M. R. Haberman, and A. Alú, Cancellation of the acoustic field scattered from an elastic shere using periodic isotropic elastic layers, J. Acous. Soc. Am. **85**, 2374 (2010).

[20] V. M. García-Chocano, L. Sanchis, A. Díaz-Rubio, J. Martínez-Pastor, F. Cervera, R. Llopis-Pontiveros, and J. Sánchez-Dehesa, Acoustic cloaks by inverse design, Appl. Phys. Lett. **99**, 074102 (2011).

[21] T. Xu, X.-F. Zhu, B. Liang, Y. Li, X.-Y. Zou, and J.-C. Cheng, Scattering reduction for an acoustic sensor using a multilayered shell comprising a pair of homogeneous isotropic single-negative media, Appl. Phys. Lett. **101**, 033509 (2012).

[22] L. Sanchis, V. M. García-Chocano, R. LLopis-Pontiveros, A. Climente, J. Martinez-Pastor, F. Cervera, and J. Sánchez-Dehesa, Three-Dimensional Axisymmetric Cloak Based on the Cancellation of Acoustic Scattering from a Sphere, Phys. Rev. Lett. **110**, 124301 (2013).

[23] B. Popa, L. Zigoneanu, and S. Cummer, Experimental Acoustic Ground Cloak in Air, Phys. Rev. Lett. **106**, 253901 (2011).

[24] L. Zigoneanu, B. Popa, and S. Cummer, Three-dimensional broadband omnidirectional acoustic ground cloak, Nat. Mat. **109**, 054906 (2014).

[25] W. Kan, B. Liang, X. Zhu, R. Li, X. Zhou, H. Wu, J. Yang, and J. Cheng, Acoustic illusion near boundaries of arbitrary curved geometry, Sci. Rep. **3**, 1427 (2013).

[26] D.-Y. Ma, Potential of microperforated panel absorber, J. Acoust. Soc. Am. **104**, 2861 (1998).

[27] V. M. García-Chocano and J. Sánchez-Dehesa, Anomalous sound absorption in lattices of cylindrically perforated shells, Appl. Phys. Lett. **106**, 124102 (2015).